Astronomy 405

May 1, 2013

Interstellar Dust

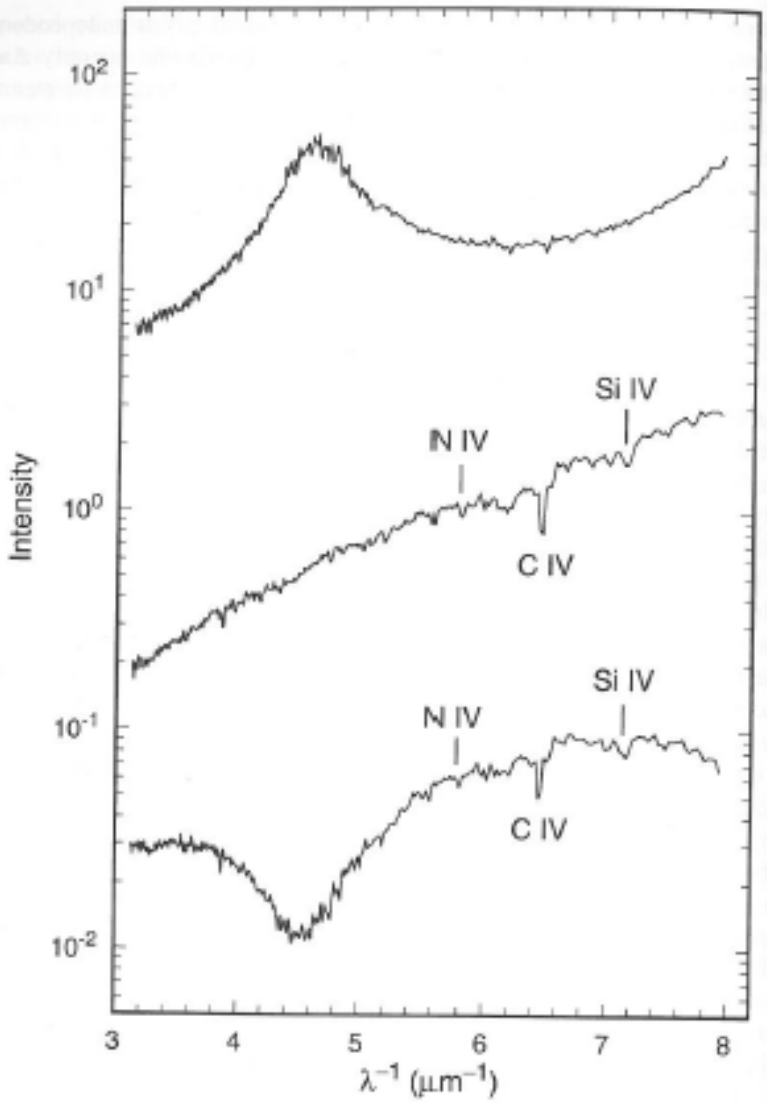

Figure 3.3. An illustration of the pair method for determining interstellar extinction curves. The lower curve is the ultraviolet spectrum of a reddened star (HD 34078, spectral type O9.5 V, $E_{B-V} = 0.54$) and the middle curve is the corresponding spectrum of an almost unreddened star of the same spectral type (HD 38666, $E_{B-V} = 0.03$). A few representative spectral lines are labelled. The vertical axis plots intensity in arbitrary units – note that the scale is logarithmic and hence equivalent to magnitude. The upper curve is the resulting extinction curve, obtained by taking the intensity ratio (equivalent to magnitude difference) of the two spectra. Based on data from the IUE *Atlas of Low-Dispersion Spectra* (Heck *et al* 1984).

Use a pair of stars, one with extinction and the other with minimal extinction.

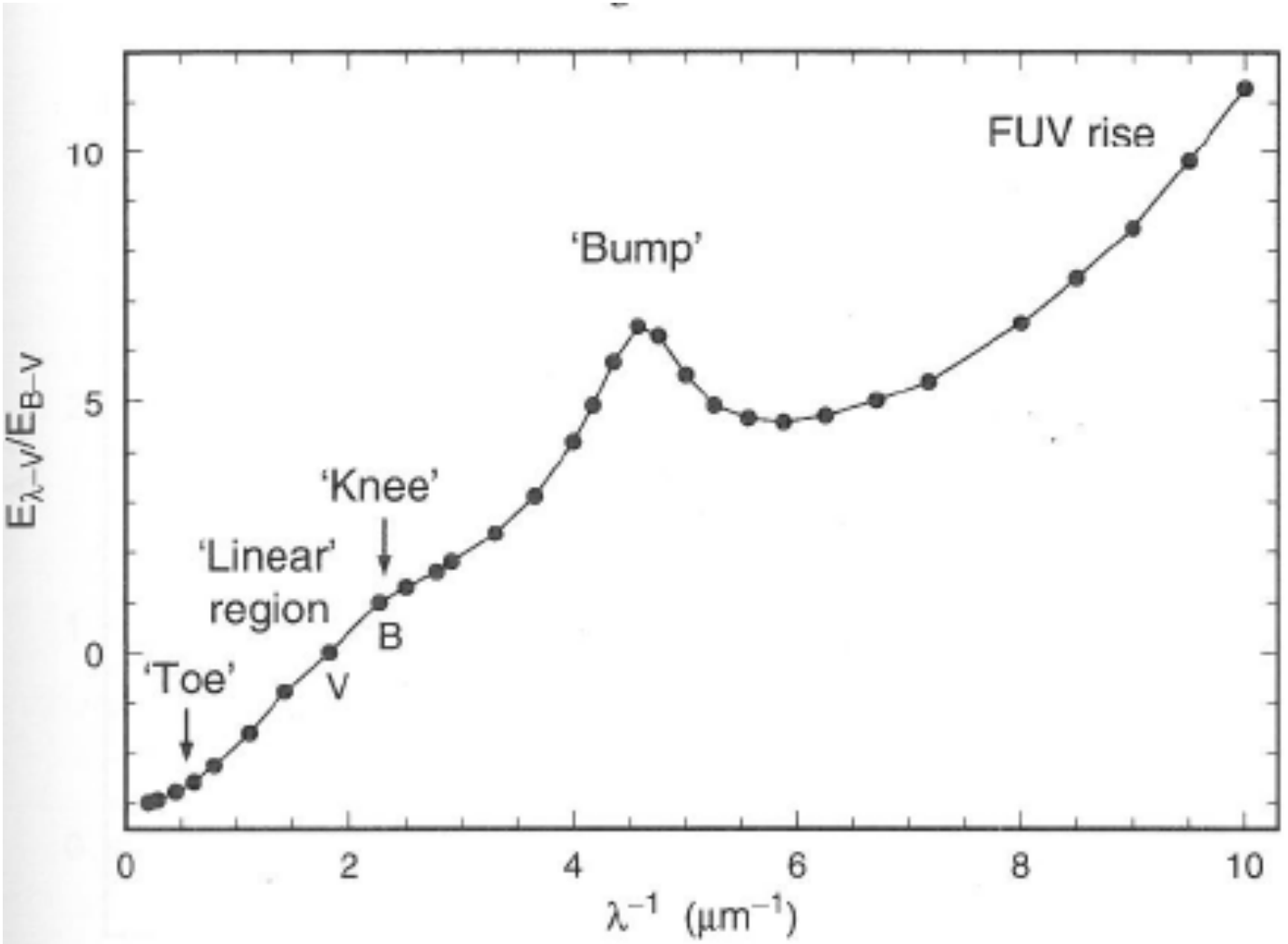

Figure 3.4. The average interstellar extinction curve ($E_{\lambda-V}/E_{B-V}$ versus λ^{-1}) in the spectral range 0.2–10 μm^{-1}. Data are from table 3.1. Various features of the curve discussed in the text are labelled. The positions of the B and V passbands selected for normalization are also indicated.

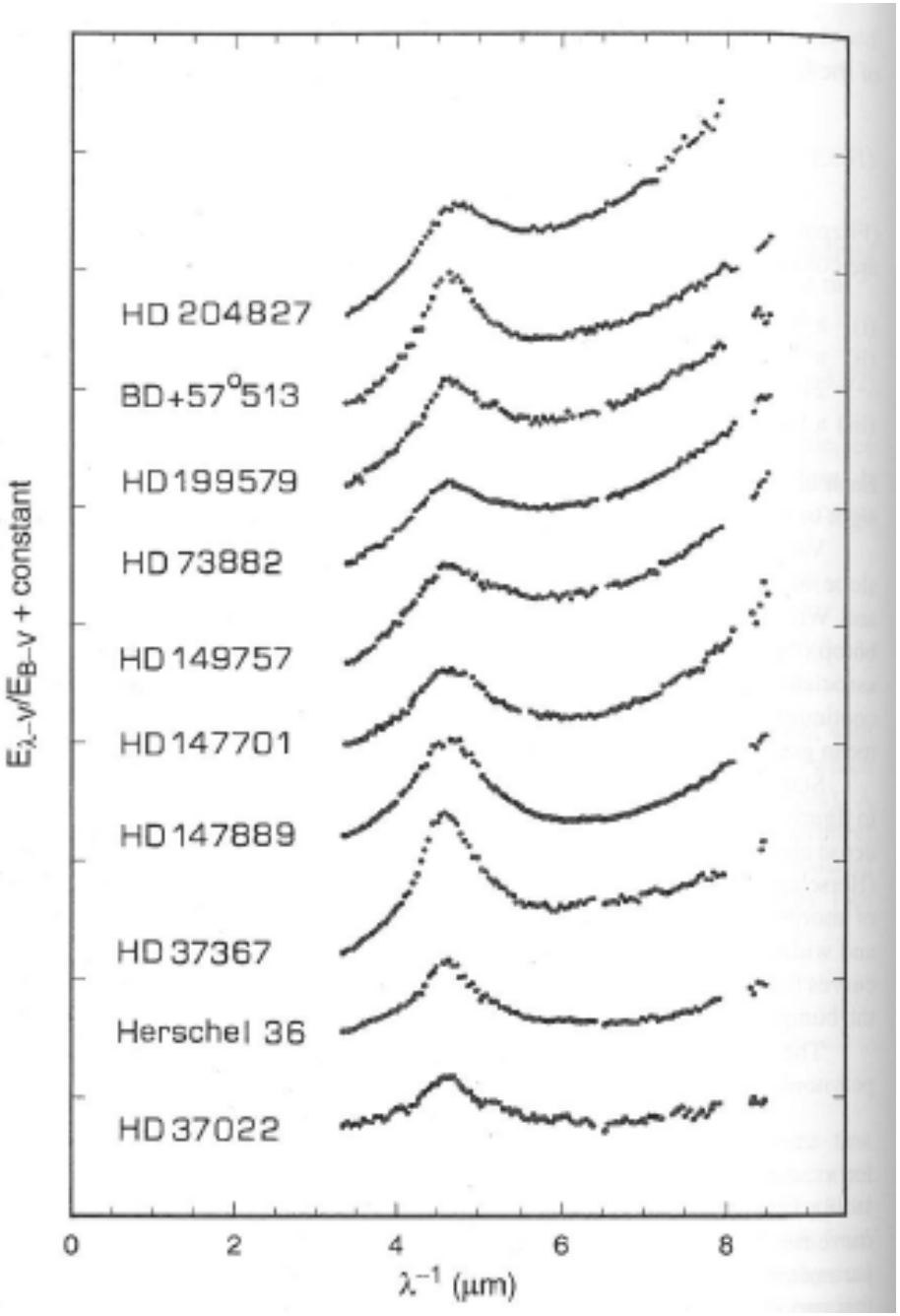
HD 204827
BD+57°513
HD 199579
HD 73882
HD 149757
HD 147701
HD 147889
HD 37367
Herschel 36
HD 37022
$E_{\lambda-V}/E_{B-V}$ + constant
0
2
4
6
8
λ^{-1} (μm)
4 mag

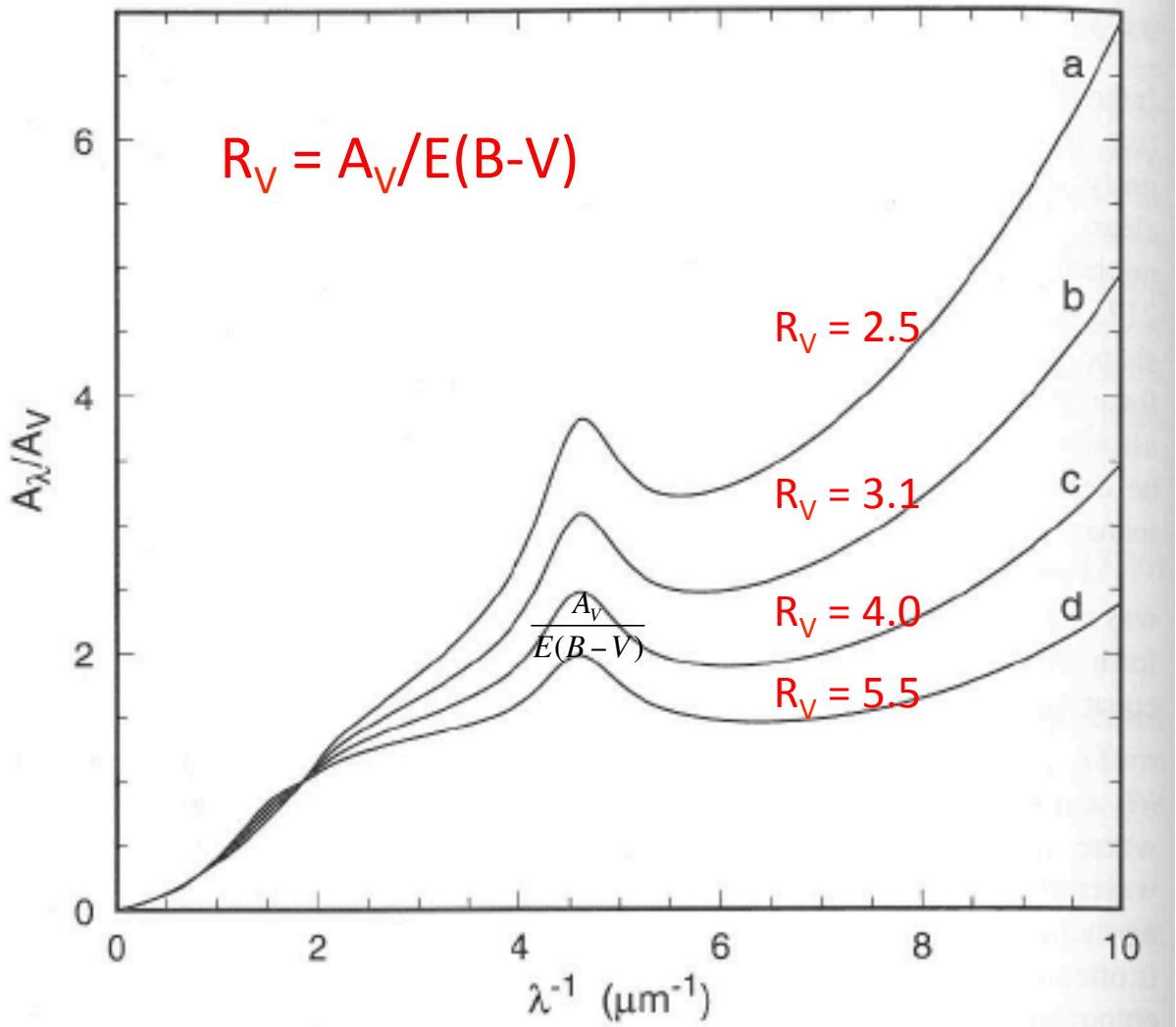

Figure 3.12. R_V-dependent variations in the extinction curve, based on empirical fits to data for many stars (originally proposed by Cardelli *et al* 1989 and shown here in the formulation of Fitzpatrick 1999): curve a, $R_V = 2.5$; curve b, $R_V = 3.1$; curve c, $R_V = 4.0$; and curve d, $R_V = 5.5$.

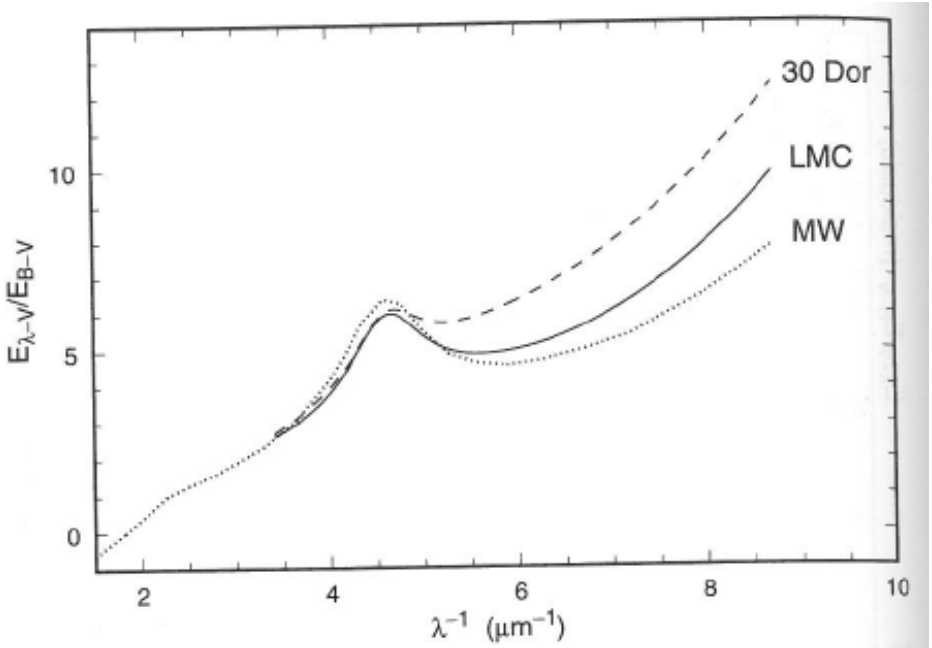

Figure 3.10. Ultraviolet extinction curves for the Large Magellanic Cloud (LMC), based on data from Fitzpatrick (1986). The average for stars widely distributed in the LMC (full curve) is compared with that for the 30 Doradus region of the LMC (broken curve) and the solar neighbourhood of the Milky Way (dotted curve; data from table 3.1).

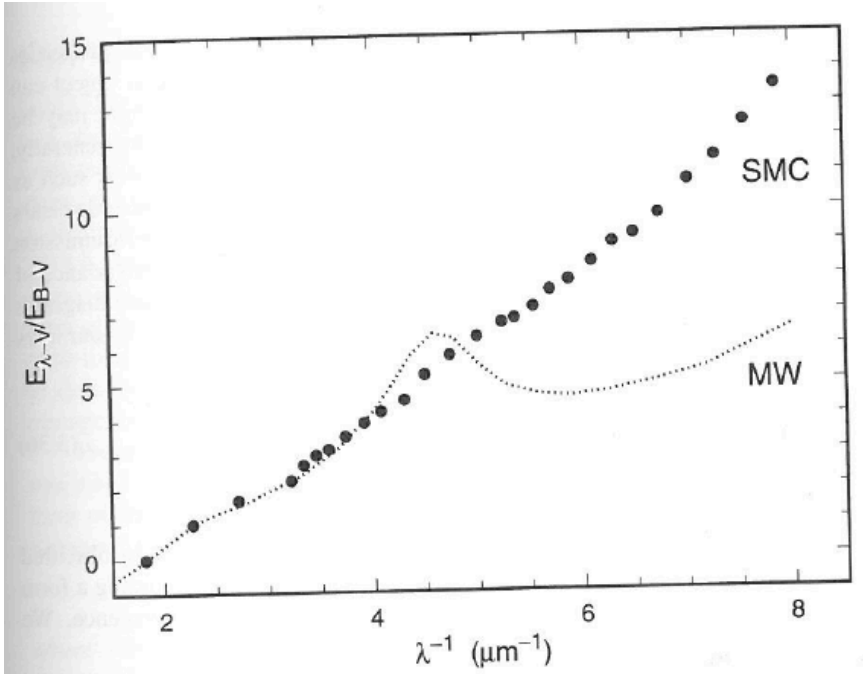

Figure 3.11. The ultraviolet extinction curve for the Small Magellanic Cloud (SMC, points; data from Prévot *et al* 1984). The average for the Milky Way is also shown for comparison (dotted curve; data from table 3.1).

Abundance effect: MW – LMC - SMC

Radiation/shock effects in 30 Dor?

Table 3.1. The average interstellar extinction curve at various wavelengths in standard normalizations. Letters in square brackets denote standard photometric passbands. Values of the coefficients $a(x)$ and $b(x)$ are also listed (see section 3.4.3).

λ (μm)	λ^{-1} (μm^{-1})	$\frac{E_{\lambda-V}}{E_{B-V}}$	$\frac{A_\lambda}{A_V}$	$a(x)$	$b(x)$
∞	0	−3.05	0.00	0.000	0.000
4.8 [M]	0.21	−2.98	0.02	0.046	−0.043
3.5 [L]	0.29	−2.93	0.04	0.078	−0.072
2.22 [K]	0.45	−2.77	0.09	0.159	−0.146
1.65 [H]	0.61	−2.58	0.15	0.230	−0.243
1.25 [J]	0.80	−2.25	0.26	0.401	−0.398
0.90 [I]	1.11	−1.60	0.48	0.679	−0.623
0.70 [R]	1.43	−0.78	0.74	0.869	−0.366
0.55 [V]	1.82	0.00	1.00	1.000	0.000
0.44 [B]	2.27	1.00	1.33	1.000	1.000
0.40	2.50	1.30	1.43	0.978	1.480
0.36 [U]	2.78	1.60	1.52	0.953	1.909
0.344	2.91	1.80	1.59	0.870	2.333
0.303	3.30	2.36	1.77	0.646	3.639
0.274	3.65	3.10	2.02	0.457	4.873
0.25	4.00	4.19	2.37	0.278	6.388
0.24	4.17	4.90	2.61	0.201	7.370
0.23	4.35	5.77	2.89	0.122	8.439
0.219	4.57	6.47	3.12	0.012	9.793
0.21	4.76	6.23	3.04	−0.050	9.865
0.20	5.00	5.52	2.81	−0.059	8.995
0.19	5.26	4.90	2.61	−0.061	8.303
0.18	5.56	4.65	2.52	−0.096	8.109
0.17	5.88	4.57	2.50	−0.164	8.293
0.16	6.25	4.70	2.54	−0.250	8.714
0.149	6.71	5.00	2.64	−0.435	9.660
0.139	7.18	5.39	2.77	−0.655	10.810
0.125	8.00	6.55	3.15	−1.073	13.670
0.118	8.50	7.45	3.44	−1.362	15.740
0.111	9.00	8.45	3.77	−1.634	17.880
0.105	9.50	9.80	4.21	−1.943	20.370
0.100	10.00	11.30	4.70	−2.341	23.500

To parametrize the extinction curve:

A_λ/A_V
$= a(x) + b(x)/R_V$

where $x = 1/\lambda$

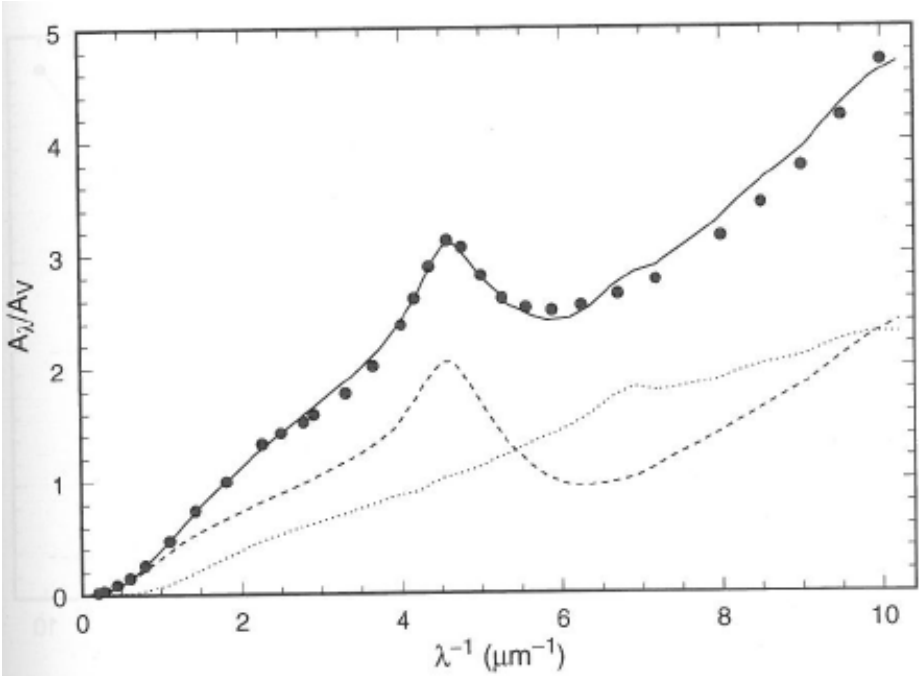

Figure 3.18. A fit to the extinction curve based on the 'MRN' two-component model (in the version of Draine and Lee 1984). The total extinction predicted by the model (continuous curve) is the sum of the contributions from graphite grains (broken curve) and silicate grains (dotted curve). The mean observational curve (table 3.1) is plotted as full circles.

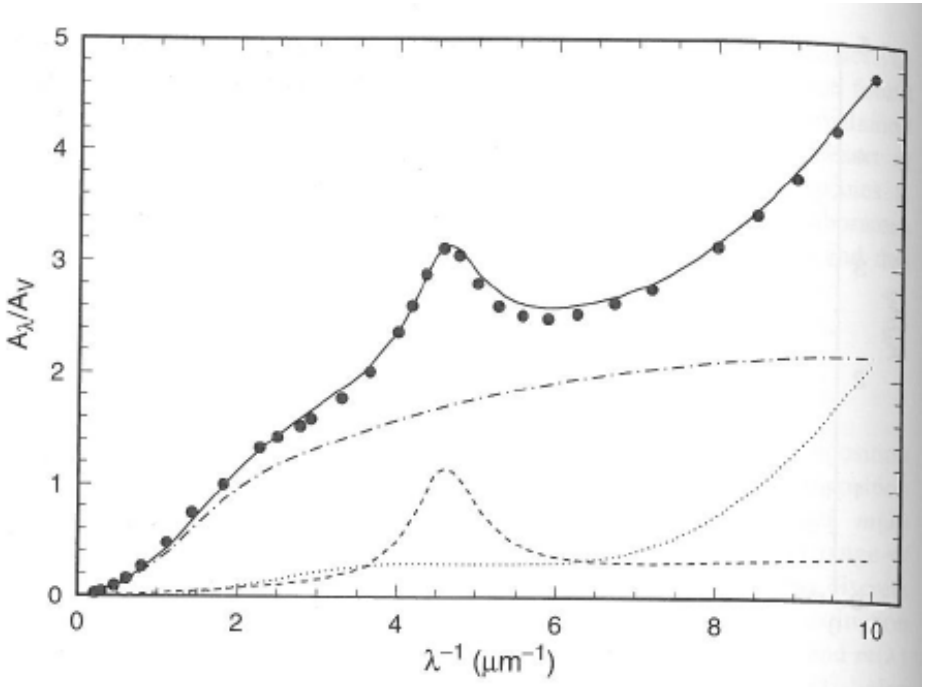

Figure 3.19. A fit to the observed extinction curve based on a three-component model (after Désert *et al* 1990). The total extinction predicted by the model (continuous curve) is the sum of the contributions from large silicate/carbon composite grains (dot–dash curve), small graphitic grains (broken curve) and PAHs (dotted curve). The mean observational curve (table 3.1) is plotted as full circles.

Diffuse Interstellar Bands (DIBs)

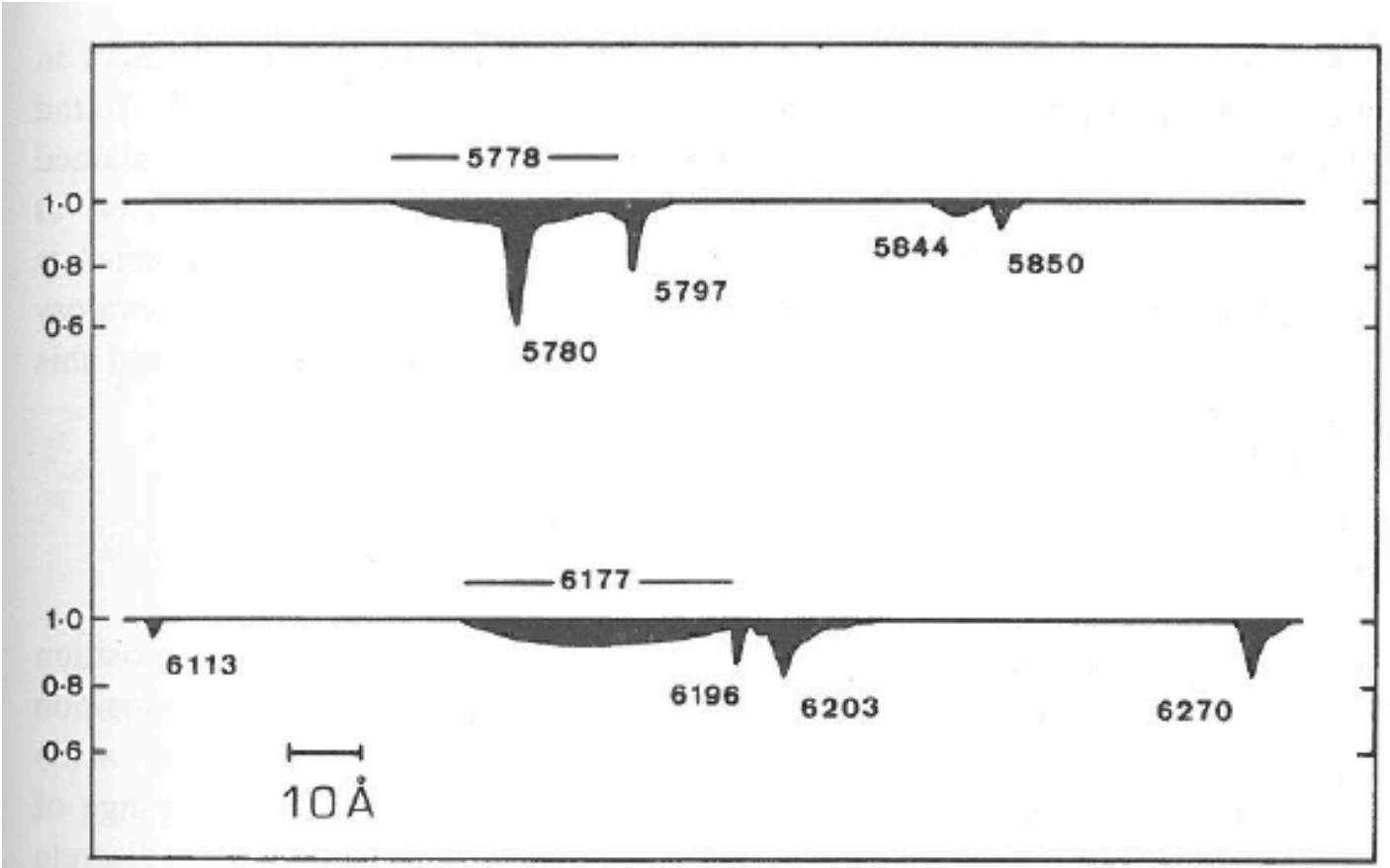

Figure 3.17. A schematic representation of diffuse bands in the yellow–red region of the spectrum, based on intensity traces for the reddened star HD 183143 (Herbig 1975). Interstellar absorptions are shown in the wavelength range 5730–5900 Å (top) and 6110–6280 Å (bottom). Photospheric and telluric features in the spectra are eliminated with reference to corresponding data for a comparison star (β Orioni) of similar spectral type and low reddening.

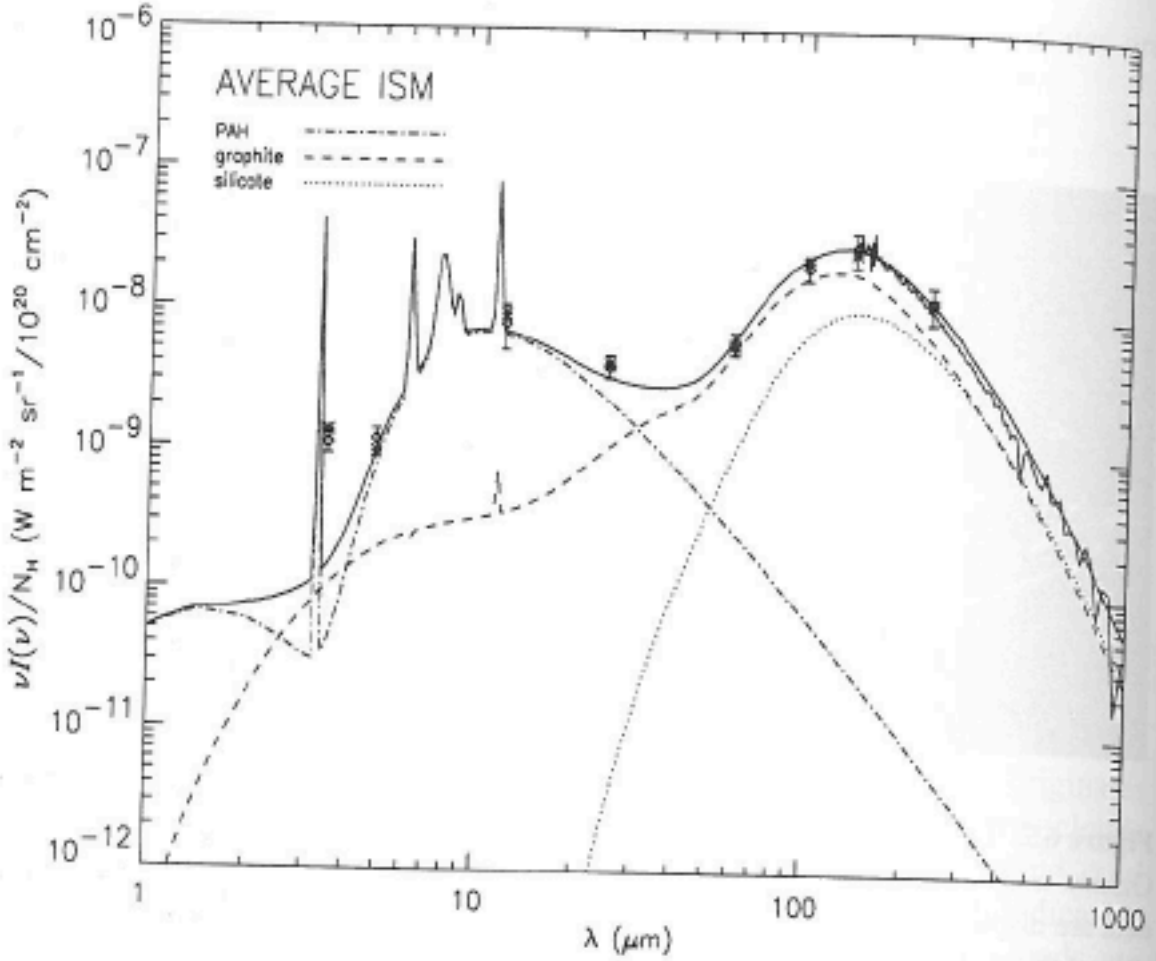

Figure 6.3. The average spectral energy distribution of diffuse emission from the diffuse ISM. The points and jagged curve represent COBE data obtained with the Diffuse Infrared Background Experiment (DIRBE) and the Far Infrared Absolute Spectrometer (FIRAS), respectively (Dwek *et al* 1997 and references therein). The continuous curve is a three-component model fit to the DIRBE data, combining emission from PAH molecules with that from uncoated graphite and silicate grains following MRN size distributions (see Dwek *et al* 1997 for details). The contribution from each individual component is also plotted. Figure courtesy of E Dwek, originally published in the *Astrophysical Journal*.

Dust emission from post-AGB Stars.

Note the broad bands of PAH emission.

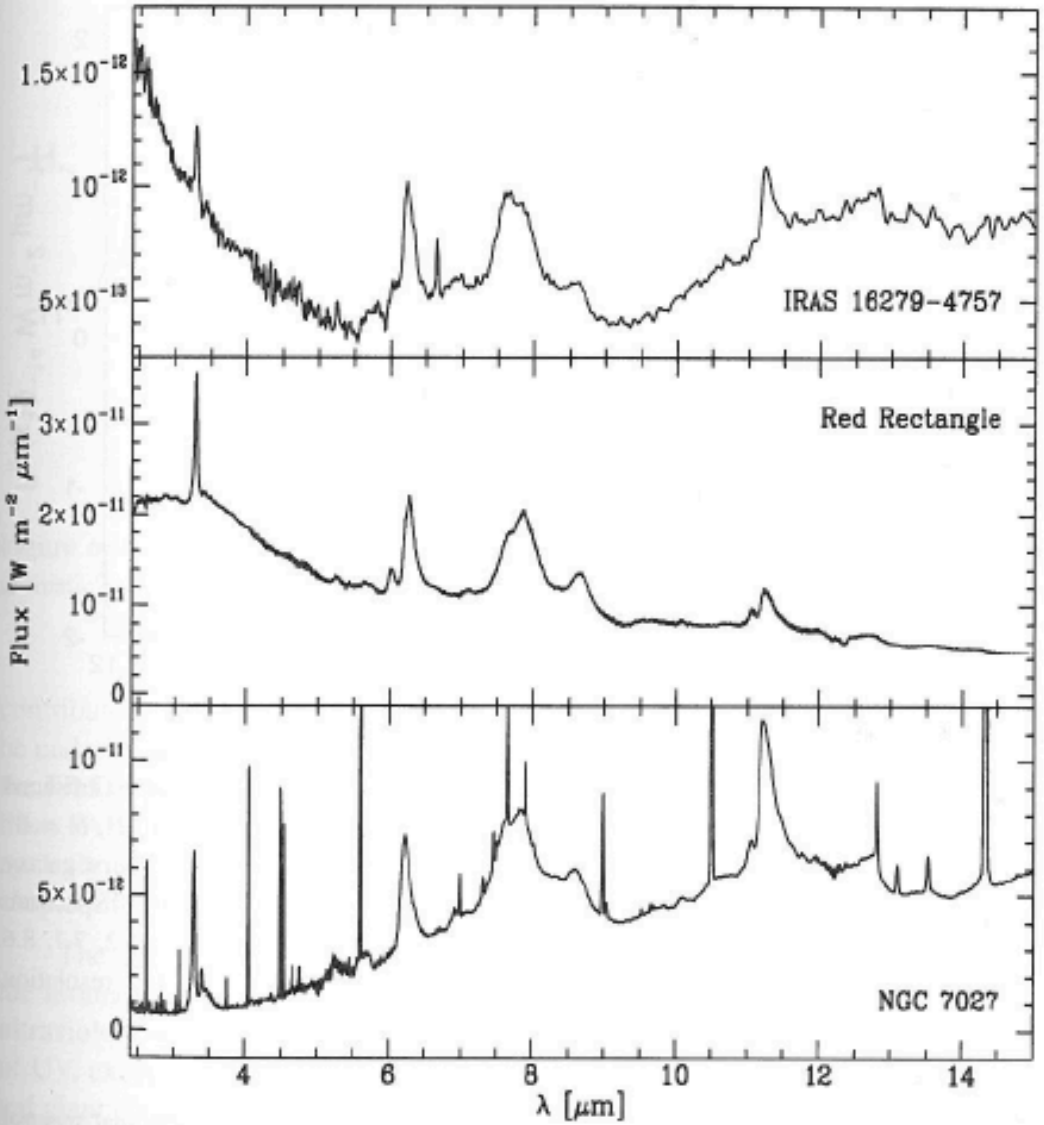

Figure 6.8. Infrared spectra of three evolved stars displaying aromatic infrared features: the post-AGB stars IRAS 16279–4757 and HD 44179 (the Red Rectangle) and the planetary nebula NGC 7027. The features listed in table 6.1 are visible in each spectrum. Additional sharp, narrow features prominent in NGC 7027 are gaseous nebular emission lines. The data were obtained with the SWS instrument on board the Infrared Space Observatory (Tielens *et al* 1999).

Polycyclic Aromatic Hydrocarbons (PAHs)

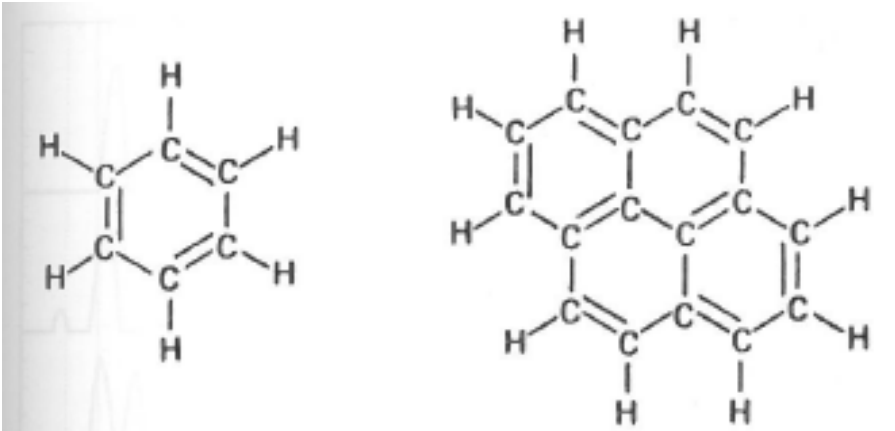

Figure 6.10. The molecular structure of benzene (left) and the four-ringed polycyclic aromatic hydrocarbon pyrene (right).

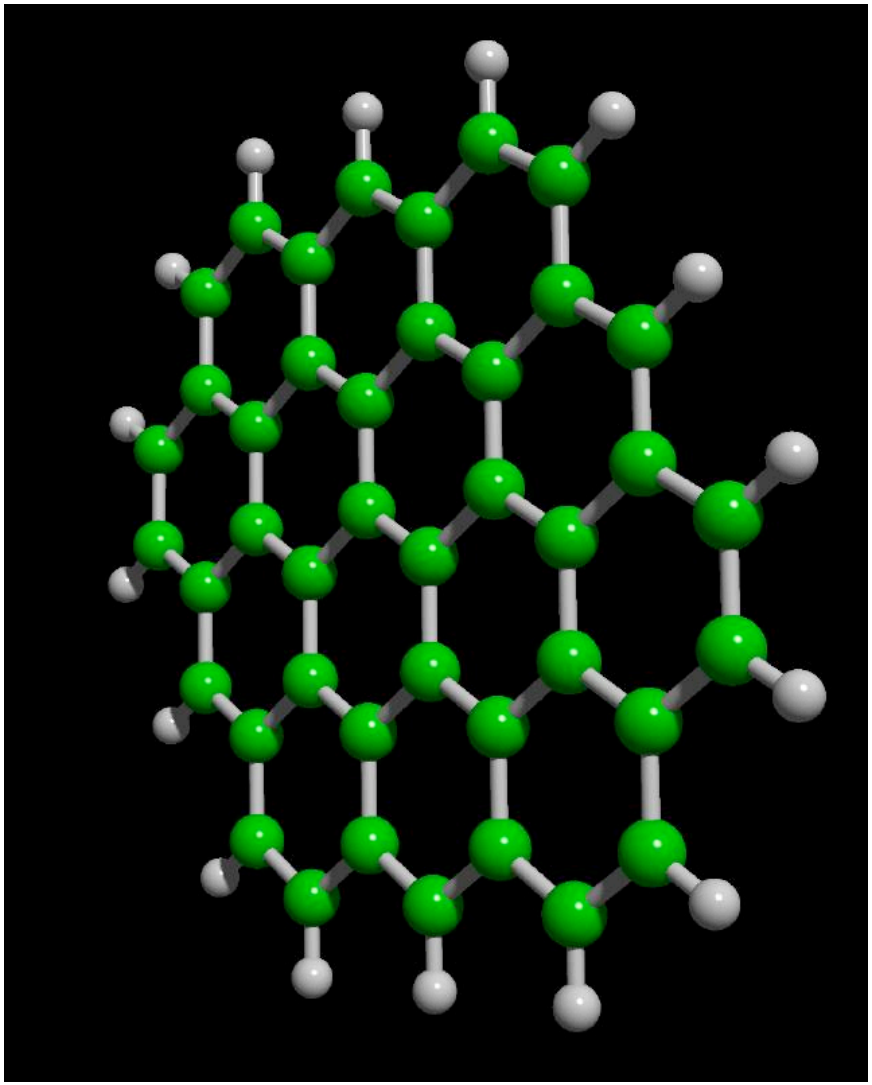

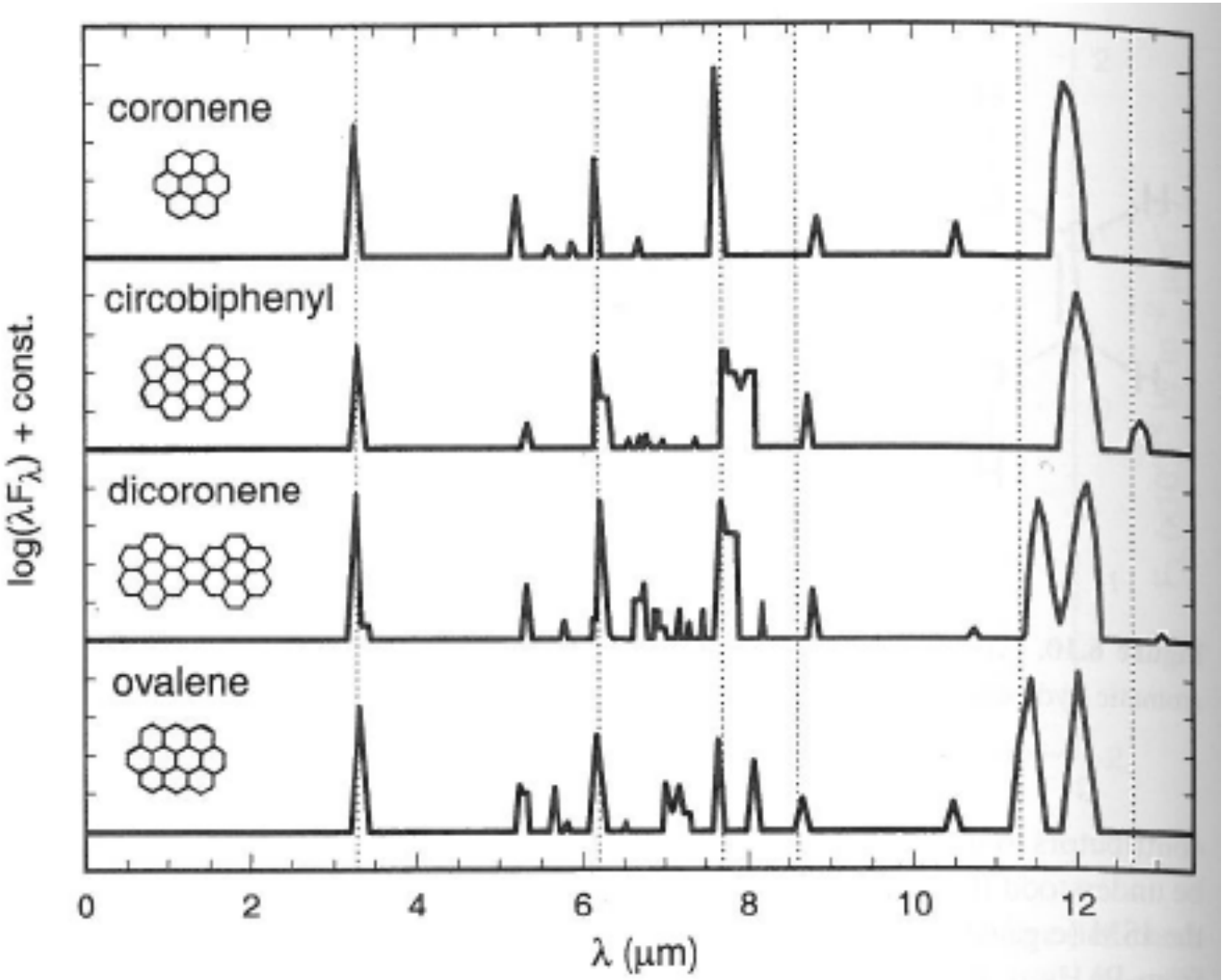

Figure 6.11. Predicted emission spectra of several PAHs at 850 K. The structure of each PAH is shown to the left of the spectrum. The vertical dotted lines indicate the positions of the principal observed features, at wavelengths 3.3, 6.2, 7.7, 8.6, 11.3 and 12.7 μm. (Adapted from Léger and d'Hendecourt 1988.)

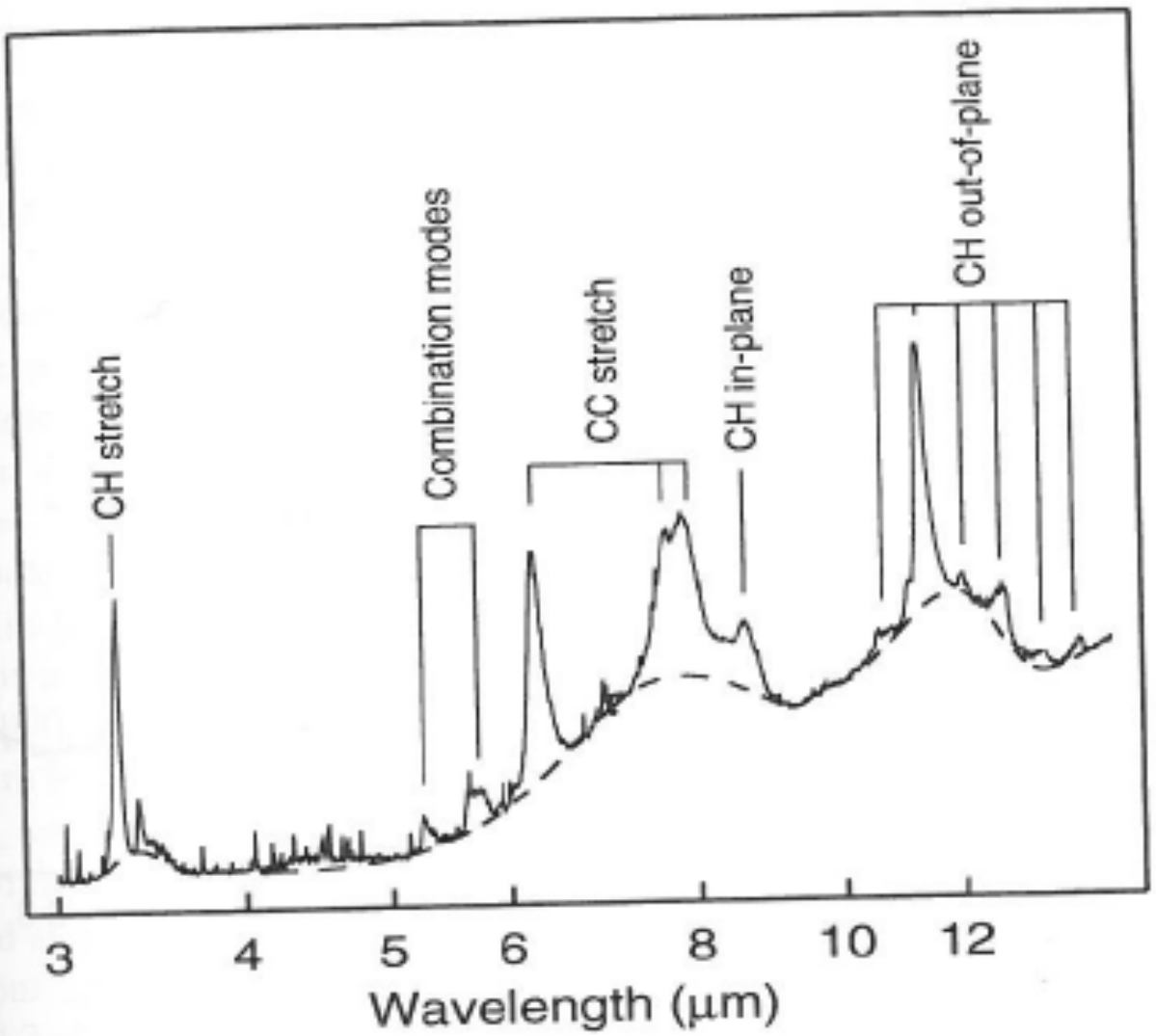

Figure 6.12. Assignment of aromatic features in the spectrum of the planetary nebula NGC 7027 to vibrational modes in PAHs. Figure courtesy of Emma Bakes, adapted from Bakes *et al* (2001).

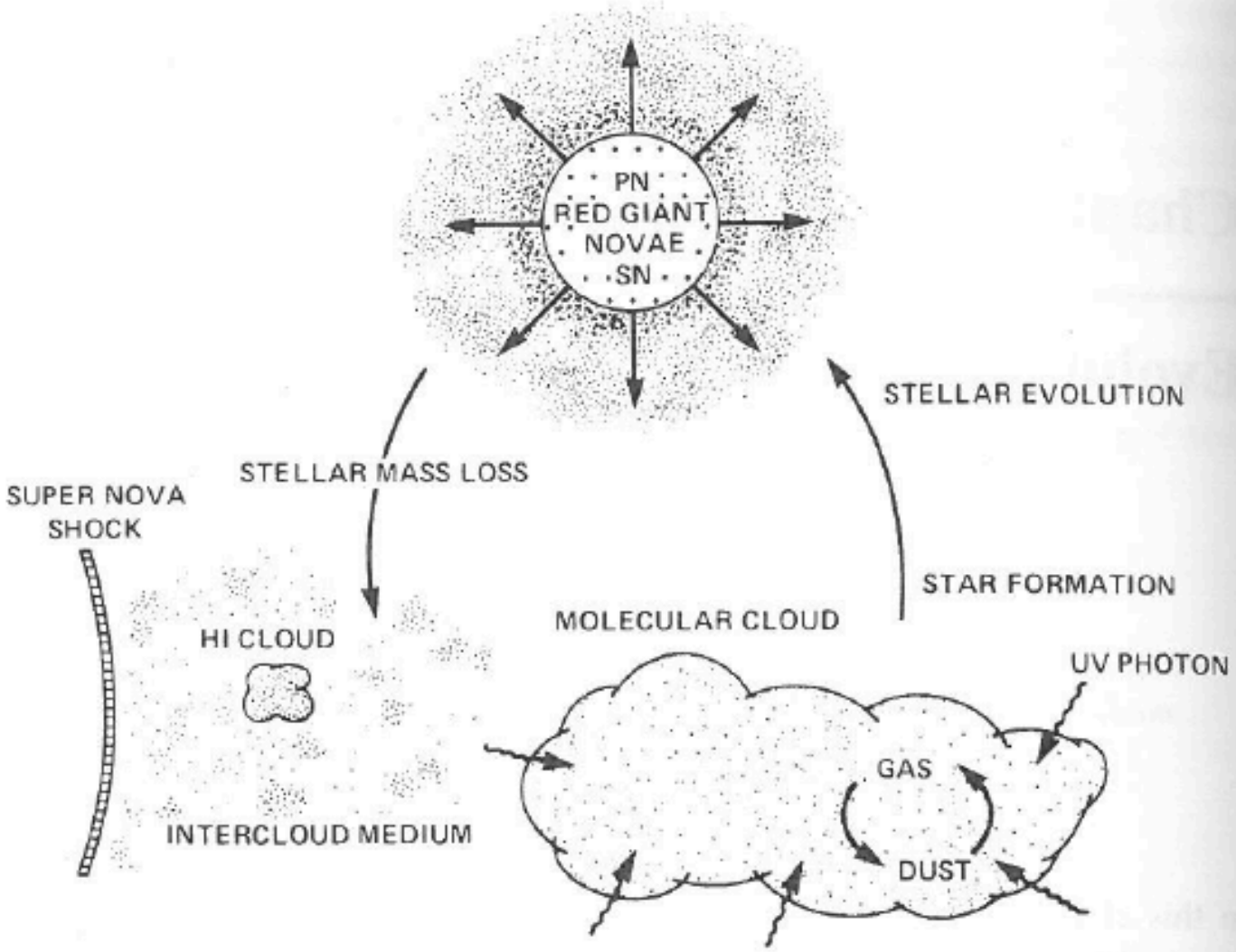

Figure 8.1. Schematic representation of the lifecycle of cosmic dust. Grains of 'stardust' originating in the atmospheres and outflows of evolved stars (red giants, planetary nebulae, novae and supernovae) are ejected into low-density phases of the interstellar medium, where they are exposed to ultraviolet irradiation and to destruction by shocks. Within molecular clouds, ambient conditions favour the growth of volatile mantles on the grains. Subsequent star formation leads to the dissipation of the molecular clouds. (From Tielens

Grain Surface Interaction to Form Molecules

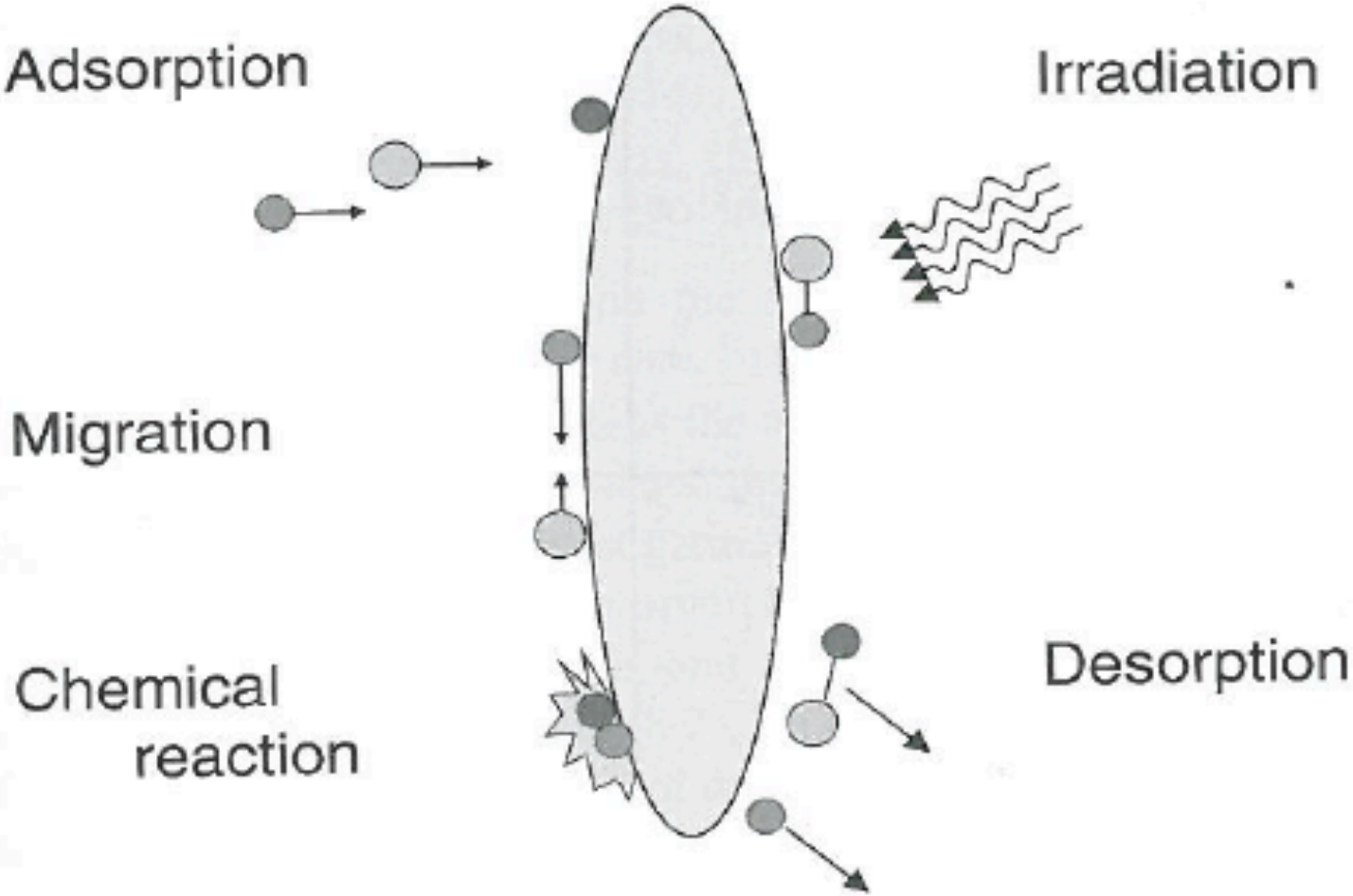

Figure 8.2. Schematic illustration of grain surface interactions. Figure courtesy of Perry Gerakines.

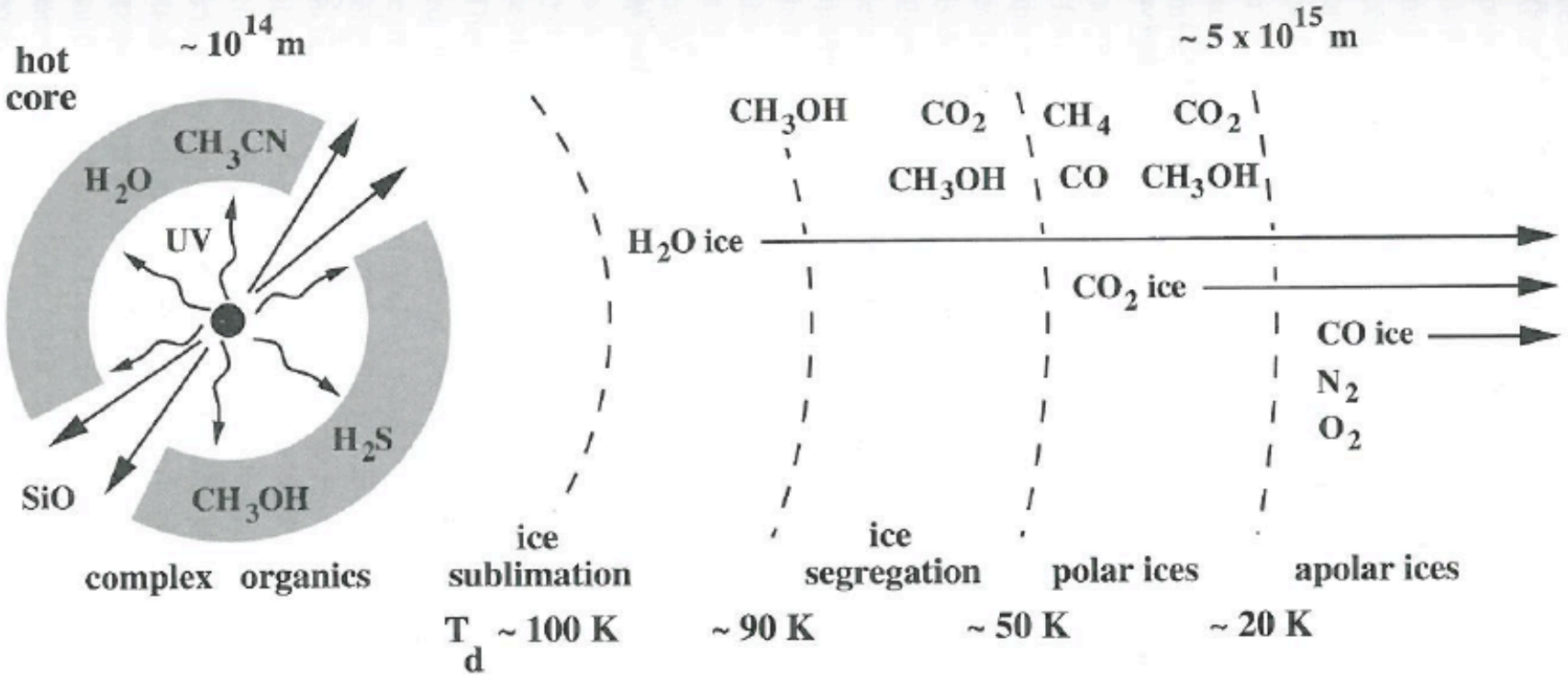

Figure 8.6. Schematic representation of the chemical environment of a massive young star embedded in a dense molecular cloud. The occurrence of various molecules in the icy mantles is indicated with respect to dust temperature (T_d) as a function of radial distance from the star. Approximate size scales are indicated for the gaseous hot core surrounding the young star and for the zone within which the apolar ices are sublimed. Figure courtesy of Ewine van Dishoeck, adapted from van Dishoeck and Blake (1998).

Table 10.1. An overview of grain components in a general model for dust in the diffuse interstellar medium.

	Silicate cores	Sooty mantles	Bump grains	Carbon VSGs
Composition	amorphous $MgSiO_3$, etc with Fe-rich inclusions	amorphous carbon	partially graphitic carbon	PAHs diamond
Origin	O-rich stardust	ISM	C-rich stardust (modified)	C-rich stardust or ISM
Size (μm)	$\leq$1	(on cores)	$\leq$0.02	~0.001
Elements depleted	O, Mg, Al, Si, Fe, etc.	C	C	C
Extinction	← UV–visible–IR →		Mid UV	Far UV
Alignment?	Yes	Yes	No	No
Polarization	← UV–visible–IR →		None	None
Absorption features	9.7, 18.5 μm	—	2175 Å 3.4 μm?	—
Emission	← FIR continuum →		← MIR continuum →	
Emission features	9.7, 18.5 μm	—	—	3.3, 6.2, 7.7, 8.6, 11.3 μm

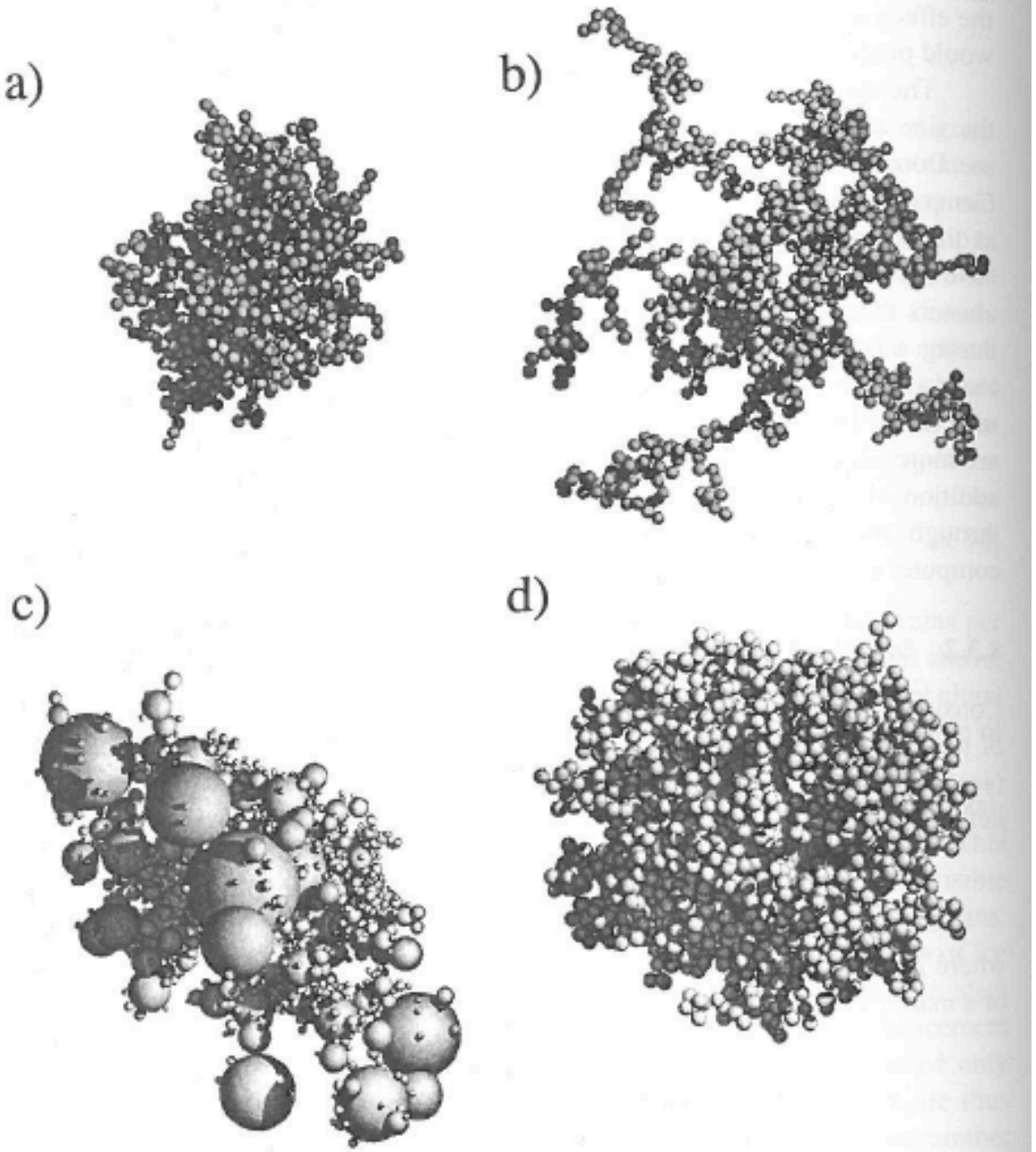

Figure 8.4. Computer simulations showing examples of particles formed by grain–grain coagulation (Dorschner and Henning 1995). (*a*) A compact particle produced by

Thank you!